Dynamic Power Management with Hybrid Power Sources*

Jianli Zhuo† Chaitali Chakrabarti† Kyungsoo Lee‡ Naehyuck Chang‡

†Department of Electrical Engineering
Arizona State University
Tempe, AZ, USA
{jianli, chaitali}@asu.edu

‡School of Computer Science and Engineering
Seoul National University
Seoul, Korea
neahyuck@snu.ac.kr

ABSTRACT

DPM (Dynamic Power Management) is an effective technique for reducing the energy consumption of embedded systems that is based on migrating to a low power state when possible. While conventional DPM minimizes the energy consumption of the embedded system, it does not utilize the properties of the power source. Alternative power sources such as fuel cells (FCs) have substantially different power and efficiency characteristics that have to be taken into account while developing policies that maximize their operational lifetime. In this paper, we present a new DPM policy for embedded systems powered by FC based hybrid source. We develop an optimization framework that explicitly considers the FC system efficiency and is aimed at minimizing the fuel consumption. Next we apply this optimization framework on top of a prediction based DPM policy to develop a new fuel-efficient DPM scheme. The proposed algorithm was applied to a real trace based MPEG encoding example and demonstrated up to 32% more system lifetime extension compared to a competing scheme.

Categories and Subject Descriptors:
D.4.7 **[Operating Systems]:** - *real-time systems and embedded systems*

General Terms: Algorithms, Design

Keywords: DPM, fuel cell, hybrid power, embedded system

1. INTRODUCTION

Embedded systems are widely used in portable computing and communication devices. Energy minimization is an important design criteria for such systems, since energy consumption determines the operational lifetime of these systems.

Dynamic power management (DPM) is an effective and well-known technique to reduce energy consumption at the system level. The key here is to put the device into a low power state when the idle time is long. Research in this area includes prediction of future idle periods [1, 2, 3], stochastic control [4, 5], aggregation of small idle times to get longer idle durations [6, 7], etc. Future idle period prediction policies are based on past history using linear function [1], regression function [2], or adaptive learning tree [3]. The stochastic control techniques are based on probabilities of different actions that are calculated using the Markov chain model [4, 5]. In order to fully utilize DPM, techniques based on aggregation of small idle slots are particularly useful, such as the task procrastination algorithm in [6], and the task scheduling algorithm for a multiple device system in [7].

While existing power management strategies aim at energy minimization of the embedded systems, they do not consider the characteristics of the power source. As a result, the minimum energy consumption of the embedded system does not necessarily transform to the maximum lifetime of the overall system. Notable exceptions are the battery-aware power management strategies that explicitly take into account the battery non-linearities by battery scheduling [5] and load profile shaping [8].

Now consider an embedded system that is powered by a non-traditional power source, such as the fuel cell (FC). FCs have attracted a great deal of attention because an FC package is expected to generate power longer (4 to 10X) than a battery package of the same size and weight. However, the power and efficiency characteristics of the FC are quite different from batteries. While both FCs and batteries have higher efficiencies for lower load currents, the variation in efficiency is much stronger for the FC. Moreover, FCs have no recovery effect. Thus battery-aware DPM policies cannot be applied to FC systems.

A stand-alone FC system is also not a viable option. FCs have limited power capacity, i.e., their power range is limited. Thus a hybrid power source composed of an FC that has high energy density and a secondary power source (such as battery or super capacitor) with high power density is much more efficient [9, 10].

In our previous work, we have developed DVS algorithms for embedded systems powered by FC-based hybrid sources. We have considered the case when the FC works at fixed output level [10] and the case when the FC supports multiple output levels [11]. In both cases, we have demonstrated that the FC lifetime is maximized by minimizing the energy delivered from the power source and not just minimizing the energy consumed by the embedded system.

In this paper, we describe a fuel-efficient DPM policy which aims at maximizing the operational lifetime of the FC by jointly applying DPM on the embedded system and fuel-efficient current setting of the power source. Maximizing the lifetime of the FC is equivalent to minimizing the fuel consumption in a given time. We determine FC output setting by utilizing an optimization framework that considers the FC system efficiency characteristics explicitly. For run time operation, we propose the fuel-efficient DPM algorithm, *FC-DPM*, which applies the optimal FC output setting policy

*This work was partly supported by the Consortium for Embedded Systems (Arizona State University), and LG Yonam Research Foundation. The research facilities were supported by ICT at Seoul National University.

DAC 2007, June 4–8, 2007, San Diego, California, USA.

to a conventional DPM prediction policy. To the best of our knowledge, this paper is the first DPM work on FC powered embedded systems. The main contributions of this paper are as follows:

- Measured and characterized the FC system efficiency according to its output current.
- Proposed an optimization framework that explicitly considers the FC system efficiency and is aimed at minimizing the fuel consumption.
- Developed a new fuel-efficient DPM algorithm, that is built on top of a prediction based DPM policy and utilizes the optimization framework.
- Applied the DPM algorithm on real trace based MPEG encoding example running on a DVD camcorder, and demonstrated up to 24.4% fuel consumption saving, which is equivalent to 32% lifetime extension.

The rest of the paper is organized as follows: The FC system and its efficiency characteristics are introduced in Section 2. Section 3 presents an optimization framework for determining the FC system output that minimizes fuel consumption for a given load profile. Section 4 presents an online DPM algorithm based on this framework. Experimental results with MPEG encoding/recording traces are given in Section 5, and the paper is concluded in Section 6.

2. FC SYSTEM AND ITS EFFICIENCY

2.1 FC hybrid power source

The system under study is an embedded system that is powered by an FC hybrid power source as shown in Figure 1.

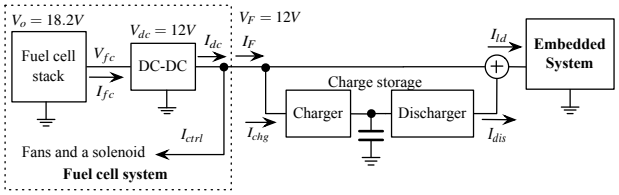

Figure 1: Block diagram of the FC hybrid system.

The FC system includes the FC stack, the DC-DC converter, and the controller. The FC stack is built with 20 cells and has an open circuit voltage V_o=18.2V. The output of the FC stack (denoted as V_{fc} and I_{fc}) is regulated by the DC-DC converter, and is used to power the embedded system and the controller. The DC-DC converter is of type PWM-PFM: it acts in the PWM (pulse width modulation) mode when its output current is high and switches to PFM (pulse frequency modulation) mode when the output current is small. Such a converter has very high efficiency ($\sim 85\%$) for the entire load range. The controller includes a cathode air blow fan, a cooling fan, a purge valve solenoid, and a microcontroller.

The output of the FC system is denoted by voltage V_F and current I_F: V_F is the same as the DC-DC output voltage V_{dc} which is 12V; $I_F = I_{dc} - I_{ctrl}$, where I_{dc} is the DC-DC output current and I_{ctrl} is the controller current.

The charge storage element acts as a buffer between the FC system output current I_F and the embedded system load current I_{ld}: it is charged by $I_{chg} = I_F - I_{ld}$ when $I_{ld} < I_F$ and is discharged by $I_{dis} = I_{ld} - I_F$ when $I_{ld} > I_F$. The charge storage could be implemented by either a Li-ion battery or a super capacitor.

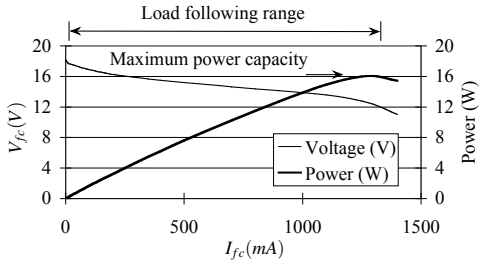

Figure 2: Measured FC stack voltage (V_{fc}) and power versus stack current (I_{fc}) characteristics of the BCS 20 W, 20 stack, room-temperature hydrogen FC (@2 psig H_2 pressure).

2.2 Fuel cell basics

An FC stack has two electrodes (anode and cathode) separated by an ion conducting membrane. H_2 is fed at the anode and splits into H^+ and e^-. The H^+s move towards the cathode through the membrane and the e^-s find a path to the cathode through the external circuit thus performing electrical work. O_2 fed at the cathode reacts with H^+ and e^- to produce H_2O as a byproduct.

The I-V-P curve in Figure 2 shows the output characteristics of the BCS 20W FC stack under consideration. The current I_{fc} is changed by controlling the fuel flow rate in the stack. As the current I_{fc} increases, the stack voltage V_{fc} decreases, and the output power $V_{fc} \times I_{fc}$ first increases and then decreases. The maximum output power point determines the power capacity, and also the extent of the load following range of the FC stack.

If we use the FC alone, the load following range in Figure 2 has to be large enough to handle the peak load power, which results in a very pessimistic use of the FC stack in terms of weight and volume. If, however, we utilize a hybrid power source as shown in Figure 1, the peak power demand can be handled by the charge storage device. In such a case, the FC size can be chosen based on the average load, which is a lot smaller.

2.3 FC system efficiency

The FC system efficiency, η_s, is defined as the FC system output power, $V_F \times I_F$, divided by Gibbs free energy per second (denoted as ΔE_{Gibbs}) [12]. ΔE_{Gibbs} is proportional to the fuel flow rate. Since the fuel flow rate is proportional to I_{fc}, we have $\Delta E_{Gibbs} = \zeta \times I_{fc}$. Therefore, η_s is given by

$$\eta_s = \frac{V_F \times I_F}{\Delta E_{Gibbs}} \propto \frac{V_F \times I_F}{\zeta \times I_{fc}}, \quad (1)$$

and η_s is affected by the FC stack efficiency, the DC-DC converter efficiency and the loss due to the controller current.

The FC stack efficiency is defined by the stack output power divided by ΔE_{Gibbs}, that is $\frac{V_{fc} \times I_{fc}}{\zeta \times I_{fc}} = \frac{V_{fc}}{\zeta}$. Thus the stack efficiency follows the same trend as the stack output voltage (see Figure 2). The measured FC stack efficiency is shown in Figure 3(a).

If we use a PWM DC-DC converter and a controller designed by a constant-speed cathode air blow fan and an on/off controlled cooling fan, the measured FC system efficiency is shown in Figure 3(c). The FC system efficiency can be treated as a constant in the load following range 0.3 A-1.2 A (the efficiency variation is within ± 3). This is the configuration that was used in [10, 11].

In this paper, we use a PWM-PFM DC-DC converter and a variable-speed fan, where the fan speed is proportional to the load current. This is a more sophisticated configuration and the measured FC system efficiency is now higher as shown in Figure 3(b). Here the FC system efficiency is a function of the FC system output current.

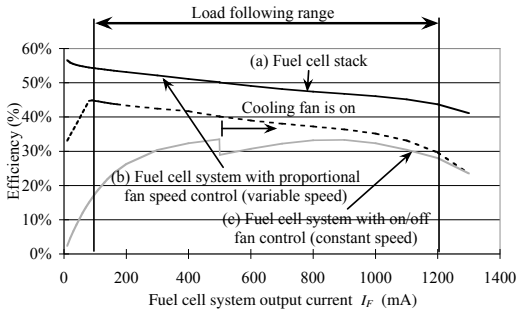

Figure 3: Measured FC stack efficiency and FC system efficiency versus the FC system output current.

In the load following range under consideration ($I_F \in [0.1A, 1.2A]$), η_s can be characterized by a simple linear model

$$\eta_s \approx \alpha - \beta I_F, \tag{2}$$

where α and β are positive coefficients determined by the measured efficiency curve. In our setup, $\alpha = 0.45$ and $\beta = 0.13$.

The relation between I_{fc} and I_F can be derived from Equation (1) and (2), and expressed as

$$I_{fc} = \frac{V_F \times I_F}{\zeta \times \eta_s} = \frac{V_F \times I_F}{\zeta \times (\alpha - \beta I_F)}. \tag{3}$$

Since $V_F = 12$V, and from out measurement, $\zeta \approx 37.5$, we have

$$I_{fc} = 0.32 \times \frac{I_F}{\eta_s} = \frac{0.32 \times I_F}{\alpha - \beta I_F}. \tag{4}$$

3. OPTIMAL FC CURRENT SETTING

The goal is to maximize the lifetime of the FC for a given fuel amount. This is equivalent to minimizing the fuel consumption. In this section, we present an optimization framework to determine the FC current to achieve this goal. We assume that the load current profile has already been generated by a DPM policy.

3.1 Definitions

The DPM-enabled embedded system has three power modes: RUN, STANDBY, SLEEP. The current in the RUN mode is dependent on the task specification, while the currents in the STANDBY mode and the SLEEP mode are denoted by I_{sdb} and I_{slp}, respectively and are system specific. The transition delay overhead when entering the SLEEP mode is τ_{PD} (PD - power down), and the corresponding current value is I_{PD}. The overhead when exiting the SLEEP mode are delay τ_{WU} (WU - wake up) and current I_{WU}. Note that we only consider the current parameters since the output voltage of the DC-DC converter is a constant (12V in this paper).

The load timing profile of the embedded system is specified by a sequence of task slots; each task slot consists of an idle period (no task request) followed by an active period (with task request). For a given task slot, the length of the idle period is denoted as T_i, and the length of the active period is T_a. In the idle period (active period), the embedded system load current is $I_{ld,i}$ ($I_{ld,a}$), the FC system output current is $I_{F,i}$ ($I_{F,a}$), and the FC stack current is $I_{fc,i}$ ($I_{fc,a}$). The power state of the embedded system during the idle period could be either STANDBY or SLEEP, depending on the length of the idle period. Consequently, $I_{ld,i}$ could be either I_{sdb} or I_{slp}. Recall that to enter the SLEEP mode, the idle period has to be longer than the DPM break-even time T_{be} [4].

In order to refer to a specific task slot, we add an extra index term: for example, $T_i(k)$ stands for the length of the idle period of the k-th slot (also referred to as k-th idle slot).

The charge storage element has a capacity C^{max}. The state of this storage element is C_{ini} at the beginning of the task slot (which is also the beginning of the idle slot), and is C_{end} at the end of the task slot (which is also the end of the active slot).

Table 1 summarizes the definitions mentioned above.

Table 1: Definitions

I_{sdb}, I_{slp}	load current at STANDBY/SLEEP mode.
I_{PD}, I_{WU}	load current when entering/exiting SLEEP mode.
T_{PD}, T_{UW}	transition delay when entering/exiting SLEEP mode.
T_{be}	break-even time of the DPM component.
T_i, T_a	length of the idle/active slot.
$I_{ld,i}, I_{ld,a}$	load current in the idle/active slot.
$I_{F,i}, I_{F,a}$	FC system output current in the idle/active slot.
$I_{fc,i}, I_{fc,a}$	FC stack current in the idle/active slot.
α, β	the coefficients of system efficiency. $\alpha = 0.45$, $\beta = 0.13$.
C^{max}	capacity of the charge storage element.
C_{ini}, C_{end}	stored charge at the beginning/end of the task slot.

3.2 Motivational example

Assume that the load current profile in a given task slot is defined by T_i=20 s with $I_{ld,i}$=0.2 A, and T_a=10 s with $I_{ld,i}$=1.2 A. The capacity of the charge storage element is C^{max}=200 A-s.

We use three different methods to determine the FC output for this load current profile.

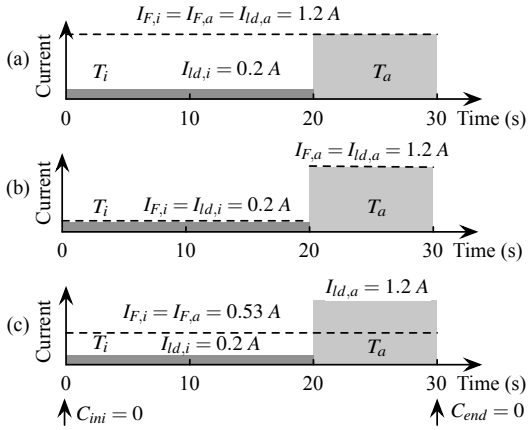

Figure 4: Different FC output for a given load profile: (a) FC system output current is fixed (*conv-DPM*), (b) FC system output follows the load faithfully (*ASAP-DPM*), and (c) the most efficient FC system output current setting (*FC-DPM*).

Setting (a) or *conv-DPM*: We do not apply any FC output control; the FC system has to constantly deliver the current corresponding to the highest load current profile. As shown in Figure 4(a), $I_{F,i} = I_{F,a}$ =1.2 A, and thus the FC current is $I_{fc,i} = I_{fc,a}$ =1.3 A according to Equation (4). The fuel consumption is proportional to $I_{fc,i} \times T_i + I_{fc,a} \times T_a = 36$ A-s.

Setting (b) or *ASAP-DPM*: We control FC system output and match it with the load profile perfectly, as shown in Figure 4(b). The FC system output current is now $I_{F,i}$ =0.2 A during the idle period, and $I_{F,a}$ =1.2 A during the active period. The corresponding values of I_{fc} are 0.15 A and 1.3 A, respectively, and the fuel consumption is proportional to $I_{fc,i} \times T_i + I_{fc,a} \times T_a = 16$ A-s.

Setting (c) or *FC-DPM*: We utilize the charge storage element, and set the FC system current to $I_{F,i} = I_{F,a}$ =0.53 A. The charge storage is charged to 10.67 A-s during the idle slot, and discharged to 0 after the active slot. The profile is shown in Figure 4(c). The

corresponding I_{fc} is 0.448 A, and the fuel consumption is proportional to $I_{fc,i} \times T_i + I_{fc,a} \times T_a = 13.45$ A-s, which is 62.6 % lower than Setting (a), and 15.9 % lower than Setting (b).

While the energy delivered from the FC system in Setting (b) and (c) are the same ($V_F \times (I_{F,i}T_i + I_{F,a}T_a) = 192$ J), the fuel consumption in Setting (c) is 15.9 % lower than that of Setting (b). In the next section, we describe a formal procedure to derive the most fuel efficient I_{fc} setting which exploits the difference in the FC system efficiencies (η_s) at different FC system output current (I_F) levels.

3.3 Determining the fuel-efficient I_{fc}

In this section, we describe the optimization process for determining the fuel-efficient I_{fc} for a single task slot. We make the following assumptions: (1) the FC output only changes when there is a power state transition on the embedded system; (2) there is no charging/discharging loss in the charge storage element.

3.3.1 No DPM state transition overhead

We begin with a relatively simple case where the DPM state transition overhead (time, energy) is ignored. The objective function that we want to minimize is the fuel consumption, which is proportional to the product of the FC stack current and the length of the corresponding duration, i.e., $I_{fc,i} \times T_i + I_{fc,a} \times T_a$. According to the relationship between I_{fc} and I_F in Equation (4), the objective function is given by

$$\min : O(I_{F,i}, I_{F,a}) = \frac{I_{F,i}}{\alpha - \beta I_{F,i}} \times T_i + \frac{I_{F,a}}{\alpha - \beta I_{F,a}} \times T_a. \quad (5)$$

First, we assume that the load following range of the FC is unlimited, and the capacity of the charge storage element is also unlimited. We further assume that we maintain $C_{end} = C_{ini}$ in each task slot for system stability. The charge stored into the charge storage element during the idle slot is given by $(I_{F,i} - I_{ld,i}) \times T_i$, and the charge delivered from it during the active slot is given by $(I_{ld,a} - I_{F,a}) \times T_a$. Based on our assumption $C_{ini} = C_{end}$, the charging amount and the discharging amount should be equal. This forms a constraint which can be written in the following form,

$$G(I_{F,i}, I_{F,a}) = (I_{F,i} - I_{ld,i}) \times T_i - (I_{ld,a} - I_{F,a}) \times T_a = 0. \quad (6)$$

The Lagrange multiplier method can be used to solve the constraint optimization problem. By introducing a factor λ, we get a new function

$$f(I_{F,i}, I_{F,a}, \lambda) = O(I_{F,i}, I_{F,a}) - \lambda \times G(I_{F,i}, I_{F,a}). \quad (7)$$

The partial derivatives of $f(I_{F,i}, I_{F,a}, \lambda)$ are

$$\frac{\partial f}{\partial I_{F,i}} = T_i \times \Big(\frac{\alpha}{(\alpha - \beta I_{F,i})^2} - \lambda \Big) = 0, \quad (8)$$

$$\frac{\partial f}{\partial I_{F,a}} = T_a \times \Big(\frac{\alpha}{(\alpha - \beta I_{F,a})^2} - \lambda \Big) = 0, \quad (9)$$

$$\frac{\partial f}{\partial \lambda} = G(I_{F,i}, I_{F,a}) = 0. \quad (10)$$

From Equation (8) and (9), we know $I_{F,i} = I_{F,a}$. Then from Equation (10), we get

$$I_{F,i} = I_{F,a} = \frac{I_{ld,i}T_i + I_{ld,a}T_a}{T_i + T_a}. \quad (11)$$

The FC stack current is calculated by substituting the value of I_F into Equation (4), i.e., $I_{fc} = \frac{0.32 \times I_F}{\alpha - \beta I_F}$.

Limited load following range: The FC load following range is limited, and expressed as $I_F \in [0.1A, 1.2A]$ for the system under consideration. Thus if $I_{F,i}$ and $I_{F,a}$ given by Equation (11) are out of range, we set them to the closest boundary value in the load following range (i.e., 0.1 A or 1.2 A).

Limited charge capacity: Next we consider the case when the capacity of the charge storage element is finite. The maximum charge that can be stored is thus bounded by C^{max}. This can be expressed by the following constraint equation,

$$C_{ini} + (I_{F,i} - I_{ld,i}) \times T_i \le C^{max}. \quad (12)$$

In this case, we still use the previous method to get $I_{F,i}$ using Equation (11) (which does not consider capacity), and then substitute $I_{F,i}$ into Equation (12) to check if the solution is valid. If the calculated $I_{F,i}$ is out of range, that is, $C_{ini} + (I_{F,i} - I_{ld,i}) \times T_i > C^{max}$, we reduce the current $I_{F,i}$ during this idle period so that $C_{ini} + (I_{F,i} - I_{ld,i}) \times T_i = C^{max}$, and then calculate $I_{F,a}$ during the active period using Equation (6). Equation (12) could be violated in the extreme case where the lower bound of the load following range is still too high. In such a case, the excess current is dissipated though the bleeder by-pass.

$C_{end} \neq C_{ini}$: If $C_{end} = C_{ini}$ for each task slot, then $C_{ini} = C_{ini}(1)$ where $C_{ini}(1)$ is the value of C_{ini} for the first task slot. However, due to factors such as limited load following range, limited charge capacity, and differences between the actual load profile and the predicted profile, C_{ini} may not be equal to $C_{ini}(1)$. For the current task slot, C_{end} is an expected value (future) and is set to $C_{ini}(1)$, while C_{ini} is a known value. The constraint in Equation (6) is now transformed to

$$C_{ini} + (I_{F,i} - I_{ld,i}) \times T_i = (I_{ld,a} - I_{F,a}) \times T_a + C_{end} \quad (13)$$

We can solve this problem by following the same method used in the case when $C_{ini} = C_{end}$.

3.3.2 Transition overhead

In order to consider the transition overhead, we make the following assumptions: (1) during the state transition, the FC output is the same as the value during the active period; (2) there is a transition between the STANDBY mode and the RUN mode in every task slot (by definition). The corresponding overhead between the STANDBY mode and the RUN mode can be absorbed into the active period by extending the length of the active period and assigning the transition current during this extended duration. With these assumptions, we only need to consider the additional overhead when the embedded system enters into the SLEEP mode.

We define a binary variable δ, where $\delta = 1$ when the embedded system is to be put into SLEEP mode during the current idle period, and $\delta = 0$ when it stays in STANDBY mode. Then the transition delay from the idle period to the active period is $\delta \times \tau_{WU}$, and the transition charge is $\delta \times I_{WU} \times \tau_{WU}$. We conservatively assume that the $(k+1)$-th idle period will be in the SLEEP mode, and take into account the transition delay τ_{PD} and charge $I_{PD} \times \tau_{PD}$ (from k-th active slot to $(k+1)$-th idle slot) into the calculation of the k-th slot.

The objective function in such a case is

$$\min : \bar{O}(I_{F,i}, I_{F,a}) = \frac{I_{F,i}}{\alpha - \beta I_{F,i}} \times T_i + \frac{I_{F,a}}{\alpha - \beta I_{F,a}} \times (T_a + \delta\tau_{WU} + \tau_{PD}),$$

and the constraint in Equation (6) is transformed to

$$C_{ini} + (I_{F,i} - I_{ld,i}) \times T_i = C_{end} + (I_{ld,a}T_a + \delta I_{WU}\tau_{WU} + I_{PD}\tau_{PD}) - I_{F,a} \times (T_a + \delta\tau_{WU} + \tau_{PD}).$$

A method similar to that outlined earlier is used to solve this optimization problem.

4. FUEL-EFFICIENT DPM

In Section 3, we described how to set the FC output such that the fuel consumption is minimized when the embedded system current profile is given. However in a real-time system, this profile changes dynamically and cannot be known a priori. In this section, we will show how to modify the conventional prediction-based DPM policy for an FC based hybrid system.

The proposed algorithm *FC-DPM* jointly controls the power state of the embedded system and the output current of the FC system such that the fuel consumption is minimized.

4.1 DPM on embedded system

Our algorithm can be built on top of any conventional DPM policy which aims at energy minimization of the embedded system. This is because a policy that reduces energy consumption does not conflict with the fuel efficient current setting, as shown below. The load energy consumption of one task slot is $\big(V_F \times (I_{ld,i} \times T_i + I_{ld,a} \times T_a)\big)$ when we ignore the transition overhead. Since V_F is a constant, if we use the policy in Section 3 to determine the FC output current, a lower energy consumption transforms to a lower I_F (according to Equation (11)), a lower I_{fc} (according to Equation (4)), and eventually a lower fuel consumption.

While we can use any existing DPM policy in our algorithm, we chose a fairly simple one which is proposed in [1]. Here the idle period duration is predicted by a linear combination of the predicted duration (denoted as T_i') and actual duration of the previous idle period, $T_i(k-1)$. The function is

$$T_i'(k) = \rho \times T_i'(k-1) + (1-\rho) \times T_i(k-1). \qquad (14)$$

If the prediction value $T_i'(k)$ is larger than the break-even time T_{be}, then the embedded system is put into the SLEEP mode.

4.2 FC system output control

In order to calculate the fuel-efficient FC output, we need information of not only the idle period but also the following active period. We propose a policy similar to [1] to get the predicted value of the active period length , T_a', by

$$T_a'(k) = \sigma \times T_a'(k-1) + (1-\sigma) \times T_a(k-1). \qquad (15)$$

The value of ρ and σ could be different, depending on the pre-known pattern of the load profile.

Once we get $T_i'(k)$ and $T_a'(k)$, we can determine the FC system output for the k-th idle slot using the method described in Section 3. After the system resumes to the active state, we re-calculate the FC system output according to the actual value of T_a and $I_{ld,a}$ of the k-th active slot.

Please note that we only mentioned how to predict the length of the active period, which is under the assumption that the current level $I_{ld,a}$ is almost constant. Actually the power consumption in different active periods could be different, and in this case, we should use an estimation value $I_{ld,a}'$, which could be set to the average load current of the past active periods.

The outline of the Algorithm *FC-DPM* is shown in Figure 5.

5. EXPERIMENTAL RESULTS

We compare the performance of Algorithm *FC-DPM* with the following algorithms:

Conv-DPM: We apply the conventional DPM policy on the FC powered system without fuel flow control. This means that the FC current is always set to $I_{fc} = 1.3$ A, corresponding to the upper bound of the load following range ($I_F = 1.2$ A).

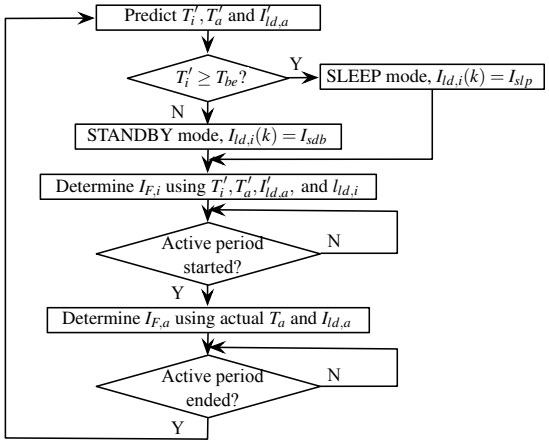

Figure 5: Outline of Algorithm FC-DPM.

ASAP-DPM: We utilize the load following capability of the FC and match the FC system output I_F to the load current I_{ld} as close as possible. The charge storage element is also used to provide additional current when the load current exceeds the load following range ($I_{ld} >$1.2 A). If the state of the charge storage drops below half its capacity, then it is recharged to full capacity as soon as possible by letting the FC deliver the highest current in the successive task slots.

5.1 Experiment 1

In our experiment, the power source consists of a BCS 20W FC stack and an 1 F super-capacitor (equivalent to 100 mA-min capacity when voltage is 12 V). The FC system efficiency coefficients based on real measurements are α=0.45 and β=0.13.

The target application is an MPEG encoding/writing task trace obtained from a DVD camcorder. The camcorder is composed of a 4X speed DVD writer, an MPEG encoder, a 16MB buffer, and an LCD (which is always off during this task trace).

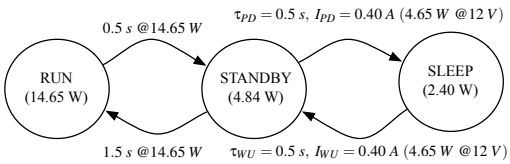

Figure 6: The power state abstraction of the DVD camcorder.

The power states and state transitions for the camcorder are shown in Figure 6, and described below:

• RUN mode: The buffer is full and the DVD writer performs the writing operation. The load power consumption is 14.65 W, and the active period length is 3.03 s (corresponding to 16 MB buffer size, and 5.28 MB/sec writing speed). The transition from STANDBY to RUN mode takes 1.5 s, and from RUN mode to STANDBY mode takes 0.5 s. The load power consumption during the state transitions is assumed to be the same as the power in the active period.

• STANDBY mode: The DVD finishes writing, and the encoder starts working. The load power consumption is 4.84 W. The length of the idle period is varied from 8 s to 20 s, depending on the characteristics of the MPEG frames.

• SLEEP mode: The encoder keeps working but the DVD is in sleep mode. The load power is 2.4 W. The state transitions from SLEEP to STANDBY and vice versa take 0.5 s and consume 4.84 W power. For such a system, the break-even time is $T_{be} = \tau_{PD} + \tau_{WU}$=1 s [4].

We apply the DPM policies for a 28 min MPEG encoding/writing task trace. The prediction factor for the idle period is set to ρ=0.5. No prediction for the active period is necessary here since the active period length is fixed.

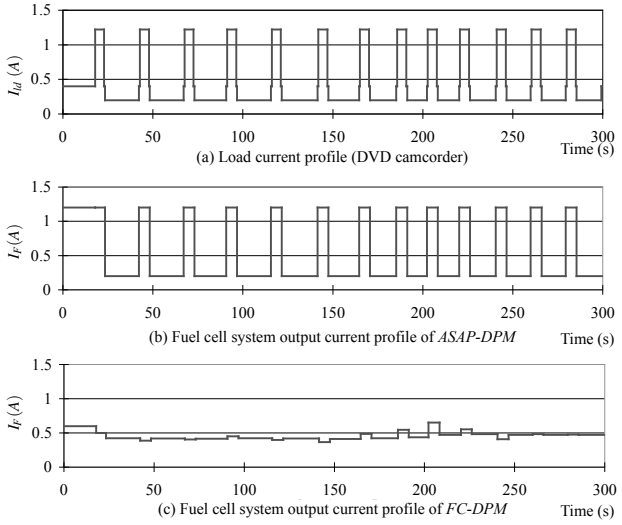

Figure 7: The current profiles of Experiment 1

Figure 7 shows 300 sec of the following current profiles: (a) the load current profile of the DVD camcorder, which is the same for all three policies, (b) the FC system output current profile (simulated) under *ASAP-DPM*, and (c) the FC system output current profile (simulated) under *FC-DPM*. We did not include the profile of *Conv-DPM* since the FC system output under this policy is always 1.2 A. As we can see from the current profiles, the load current under the *ASAP-DPM* policy follows the embedded system current very well. However, the large variation in the current during the active and the idle periods results in larger fuel consumption. The load current under policy *FC-DPM* is quite flat and results in the lowest fuel consumption due to the convexity of Equation (4).

The fuel consumptions corresponding to the different DPM policies are shown in Table 2. The values have been normalized to that of *Conv-DPM*. The fuel consumptions due to *ASAP-DPM* and *FC-DPM* are significantly lower than *Conv-DPM* because both of these policies exploit the load following capability of the power source. The algorithm *FC-DPM* reduces the fuel consumption furthermore since it determines the FC output based on its efficiency characteristics. The normalized fuel consumption of *FC-DPM* is as low as 30.8 % compared to *Conv-DPM*. If we compare *FC-DPM* and *ASAP-DPM*, *FC-DPM* saves 24.4 % more fuel. Since the lifetime is inversely proportional to the fuel consumption, *FC-DPM* has a lifetime that is higher than *ASAP-DPM* by $40.8\%/30.8\% = 1.32$.

Table 2: Normalized fuel consumption of Exp. 1

DPM policy	Conv-DPM	ASAP-DPM	FC-DPM
Compared to Conv-DPM	100%	40.8%	30.8%

5.2 Experiment 2

In this experiment, we use a synthetic embedded system profile where we bring some random factors into the DVD camcorder experiment. The idle period length is now based on a uniform distribution between [5 s, 25 s]; the active period is based on a uniform distribution between [2 s, 4 s]; the load power consumption during active period is generated by a uniform distribution between [12 W, 16 W]. The SLEEP mode transition overheads are $\tau_{PD} = \tau_{WU} = 1$ s, $I_{WU} = I_{PD} = 1.2$ A, and the break-even time is 10 s [4]. All other parameters are the same as those in the previous experiment. During prediction, we use $\rho = \sigma = 0.5$, and the future active period current $I_{ld,a}$ is estimated as 1.2 A.

The normalized fuel consumptions of the different DPM policies are shown in Table 3. The proposed algorithm *FC-DPM* still outperforms the other two competing algorithms. The savings of *FC-DPM* compared to *ASAP-DPM* is 15.5 %, which is less than the savings in Experiment 1 (24.4 %). This is because the current variances in the *ASAP-DPM* profile are smaller than that in Experiment 1, and the average current values of both algorithms are higher than in Experiment 1.

Table 3: Normalized fuel consumption of Exp. 2

DPM policy	Conv-DPM	ASAP-DPM	FC-DPM
Compared to Conv-DPM	100%	49.1%	41.5%

6. CONCLUSION

In this paper, we addressed the problem of dynamic power management for embedded systems powered by FC based hybrid power sources. Due to unique power and efficiency characteristics of the FC system, conventional DPM cannot fully achieve efficient use of the FC hybrid power source. We first characterized the FC system efficiency by real measurements. Based on the characteristics of the FC efficiency, we developed a framework to optimize fuel consumption. Next we utilized this framework on top of a prediction based DPM scheme to develop a fuel-efficient DPM algorithm, *FC-DPM*, for run time operation. The performance of Algorithm *FC-DPM* was validated on both real and synthetic MEPG decoding/writing traces. Experimental results showed up to 32 % extension of the operational lifetime compared to a competing algorithm.

7. REFERENCES

[1] C.-H. Hwang and A. Wu, "A predictive system shutdown method for energy saving of event-driven computation," in *Proc. of ICCAD*, Nov. 1997, pp. 28–32.

[2] M. Srivastava, A. Chandrakasan, and R. Brodersen, "Predictive system shutdown and other architectural techniques for energy efficient programmable computation," *IEEE Transactions on VLSI Systems*, vol. 4, pp. 42–55, 1996.

[3] EY Chung, L. Benini, and G. De Micheli, "Dynamic power management using adaptive learning tree," in *Proc. of ICCAD*, Nov. 1999, pp. 274–279.

[4] L. Benini, A. Bogliolo, and G. De Micheli, "A survey of design techniques for system-level dynamic power management," *IEEE Transactions on VLSI Systems*, vol. 8, pp. 299–316, 2000.

[5] P. Rong and M. Pedram, "Battery-aware power management based on Markovian decision processes," *IEEE TCAD*, vol. 25, pp. 1337–1349, 2006.

[6] R. Jejurikar and R. Gupta, "Leakage aware dynamic voltage scaling for real-time embedded systems," in *Proc. of DAC*, 2004, pp. 275–280.

[7] Y. Lu, L. Benini, and G. De Micheli, "Low-power task scheduling for multiple devices," in *Proc. of CODES*, 2000, pp. 39–43.

[8] L. Benini, G. Castelli, A. Macii, and R. Scarsi, "Battery-driven dynamic power management," *IEEE Design and Test of Computers*, vol. 18, pp. 53–60, 2001.

[9] L. P. Jarvis, P. J. Cygan, and M. P. Roberts, "Fuel cell/lithium-ion battery hybrid for manportable applications," in *Proceedings of the Battery Conference on Applications and Advances*, 2002, pp. 69–72.

[10] J. Zhuo, C. Chakrabarti, N. Chang, and S. Vrudhula, "Extending the lifetime of fuel cell based hybrid systems," in *Proc. of DAC*, July 2006, pp. 56–267.

[11] J. Zhuo, C. Chakrabarti, N. Chang, and S. Vrudhula, "Maximizing the lifetime of embedded systems powered by fuel cell-battery hybrids," in *Proc. of ISLPED*, Oct. 2006, pp. 424–429.

[12] J. Larminie and A. Dicks, *Fuel cell systems explained*, John Wiley & Sons, LTD, 2000.